Neurobiology of Aging 36 (2015) S113–S120

Contents lists available at ScienceDirect

Neurobiology of Aging

journal homepage: www.elsevier.com/locate/neuaging

Network and connectivity

Connectivity network measures predict volumetric atrophy in mild cognitive impairment

Talia M. Nir [a], Neda Jahanshad [a,b], Arthur W. Toga [a], Matt A. Bernstein [b], Clifford R. Jack Jr [b], Michael W. Weiner [c], Paul M. Thompson [a,d,e,f,g,h,i,*], for the Alzheimer's Disease Neuroimaging Initiative (ADNI)[1]

[a] Imaging Genetics Center, Institute for Neuroimaging and Informatics, University of Southern California, Los Angeles, CA, USA
[b] Department of Radiology, Mayo Clinic and Foundation, Rochester, MN, USA
[c] Department of Radiology and Biomedical Imaging, University of California-San Francisco School of Medicine, San Francisco, CA, USA
[d] Department of Neurology, University of Southern California, Los Angeles, CA, USA
[e] Department of Psychiatry, University of Southern California, Los Angeles, CA, USA
[f] Department of Radiology, University of Southern California, Los Angeles, CA, USA
[g] Department of Engineering, University of Southern California, Los Angeles, CA, USA
[h] Department of Pediatrics, University of Southern California, Los Angeles, CA, USA
[i] Department of Ophthalmology, University of Southern California, Los Angeles, CA, USA

ARTICLE INFO

Article history:
Received 2 May 2013
Received in revised form 13 January 2014
Accepted 17 April 2014
Available online 30 August 2014

Keywords:
Graph theory
Brain networks
White matter
DTI
Tractography
ADNI
TBM
Small worldness
Connectivity

ABSTRACT

Alzheimer's disease (AD) is characterized by cortical atrophy and disrupted anatomic connectivity, and leads to abnormal interactions between neural systems. Diffusion-weighted imaging (DWI) and graph theory can be used to evaluate major brain networks and detect signs of a breakdown in network connectivity. In a longitudinal study using both DWI and standard magnetic resonance imaging (MRI), we assessed baseline white-matter connectivity patterns in 30 subjects with mild cognitive impairment (MCI, mean age 71.8 ± 7.5 years, 18 males and 12 females) from the Alzheimer's Disease Neuroimaging Initiative. Using both standard MRI-based cortical parcellations and whole-brain tractography, we computed baseline connectivity maps from which we calculated global "small-world" architecture measures, including mean clustering coefficient and characteristic path length. We evaluated whether these baseline network measures predicted future volumetric brain atrophy in MCI subjects, who are at risk for developing AD, as determined by 3-dimensional Jacobian "expansion factor maps" between baseline and 6-month follow-up anatomic scans. This study suggests that DWI-based network measures may be a novel predictor of AD progression.

1. Introduction

Alzheimer's disease (AD), the most common form of dementia, is characterized by memory loss in its early stages, typically followed by a progressive decline in other cognitive domains. People with mild cognitive impairment (MCI), a transitional stage between normal aging and AD, convert to AD at a rate of about 10%–15% per year (Bruscoli and Lovestone, 2004; Petersen et al., 2001). The Alzheimer's Disease Neuroimaging Initiative (ADNI) is one of several major efforts worldwide to identify sensitive biomarkers that may help track or predict brain tissue loss because of AD progression.

AD is marked by pervasive gray-matter atrophy, but the brain's white-matter (WM) pathways also progressively decline (Bartzokis, 2011; Braak and Braak, 1996; Braskie et al., 2011; Hua et al., 2013). Recent models of AD suggest that cognitive deficits arise from the progressive disconnection of cortical and subcortical regions, promoted by neuronal loss and WM injury (Delbeuck et al., 2003; Pievani et al., 2011). Many magnetic resonance imaging (MRI)–based image analysis methods have been used to track structural atrophy of the brain, but diffusion weighted imaging (DWI) is sensitive to microscopic WM injury not always detectable with standard anatomic MRI. DWI may be used to track the highly

*Corresponding author at: Imaging Genetics Center, Institute for Neuroimaging and Informatics, Keck School of Medicine, University of Southern California, 2001 N. Soto St, SSB1-102, Los Angeles, CA 90032, USA. Tel.: +323 442-7246; fax:+323 442-7247.
E-mail address: pthomp@usc.edu (P.M. Thompson).

[1] Many investigators within the ADNI contributed to the design and implementation of ADNI and/or provided data, but most of them did not participate in the analysis or writing of this report. A complete list of ADNI investigators may be found at http://adni.loni.usc.edu/wp-content/uploads/how_to_apply/ADNI_Acknowledgement_List.pdf.

0197-4580/$ – see front matter © 2015 Elsevier Inc. All rights reserved.
http://dx.doi.org/10.1016/j.neurobiolaging.2014.04.038

anisotropic diffusion of water along axons, revealing microstructural WM fiber bundles connecting cortical and subcortical regions and allowing for characterization of the brain's WM structural network (Hagmann et al., 2008).

Graph theory network topology measures have been used increasingly to analyze brain networks and characterize network organization. "Small-world" network properties have been regarded as typical properties of many kinds of communication networks and are found in social networks, efficient biological networks, and in healthy mammalian brain networks (Achard and Bullmore, 2007; Hilgetag et al., 2000; Iturria-Medina et al., 2008; Reijneveld et al., 2007). Networks with a small-world organization can have both functional segregation and specialization of modules and a "low wiring cost" that supports easy communication across an entire network. Small-world networks are marked by low characteristic path length (CPL) and high mean clustering coefficient (MCC); so, they are both integrated and segregated. Studies using various modalities, including cortical thickness analyses, functional MRI, and electroencephalography, suggest that AD patients have abnormal small-world architecture in their large-scale structural and functional brain networks, with differences in MCC and CPL that may imply less optimal network topology (Brown et al., 2011; He et al., 2008; Sanz-Arigita et al., 2010; Stam et al., 2007; Toga and Thompson, 2013).

In this study, we assessed 30 ADNI participants showing signs of MCI. MCI subjects are the target for many clinical trials that aim to slow disease progression, before brain changes are so pervasive that they are irremediable. However, predictors of decline in MCI are sorely needed, as mildly impaired subjects do not usually exhibit drastic changes in most standard biomarkers of AD. Here, we combined DWI with longitudinally acquired standard anatomic MRI (across a 6-month interval) to measure the microstructure and connectivity of WM tracts and assess whether variations in the degree and extent of connections might predict future brain decline. We created 68 × 68 structural connectivity matrices, or graphs, that describe the strength of connections between any pair of brain regions based on baseline structural cortical parcellations and whole-brain tractography. In these graphs, "nodes" designate brain regions that are thought of as being connected by "edges" representing WM fibers. We then used graph theory to describe general properties of the anatomic networks and to characterize connectivity patterns.

Given the recent interest in "small-world" phenomena as a characteristic of biological networks, we examined whether global small-world architecture network measures, MCC and CPL, calculated from baseline connectivity maps were associated with "future" volumetric brain atrophy (dynamic tissue loss) over a 6-month follow-up period, as determined by 3-dimensional (3D) Jacobian "expansion factor maps" of T1-weighted structural scans. That is, we tested whether the intactness of the brain's anatomic network was associated with ongoing brain decline in the future, assessed using the more accepted anatomic MRI methods. In the follow-up analyses, we additionally assessed whether several baseline local nodal measures (efficiency [EFF], clustering, and betweenness [BTW] centrality) were associated with volumetric brain atrophy. We found that global and nodal network measures may offer a potentially useful biomarker for predicting longitudinal atrophy, at this critical time before the onset of AD.

2. Methods

2.1. Subject information and image acquisition

Data collection for the ADNI2 project (the second phase of ADNI) is still in progress. Here, we performed an initial analysis of 30 MCI subjects who had returned for a follow-up evaluation at 6 months (mean age at baseline 71.8 ± 7.5 years, 18 males and 12 females). We note that in ADNI2, MCI participants include the enrollment of a new early MCI cohort, with milder episodic memory impairment than the MCI group of ADNI1, now called late MCI in ADNI2 (Table 1). We additionally analyzed baseline data from 29 cognitively healthy control subjects to create a study-specific brain template (mean age at baseline 73.4 ± 5.2 years, 15 males and 14 females). Detailed inclusion and exclusion criteria are found in the ADNI2 protocol (http://adni-info.org/Scientists/Pdfs/ADNI2_Protocol_FINAL_20100917.pdf).

All subjects underwent whole-brain MRI scanning on 3-T GE Medical Systems scanners, on at least 1 of 2 occasions (baseline and 6 months). T1-weighted IR-FSPGR (inversion recovery fast spoiled gradient echo sequence) sequences (256 × 256 matrix, voxel size = 1.2 × 1.0 × 1.0 mm^3, inversion time = 400 ms, repetition time = 6.98 ms, echo time = 2.85 ms, and flip angle = 11°) and diffusion-weighted images (DWIs; 35-cm field of view, 128 × 128 acquired matrix, reconstructed to a 256 × 256 matrix, voxel size 2.7 × 2.7 × 2.7 mm^3, scan time = 9 minutes, and more imaging details may be found at http://adni.loni.usc.edu/wp-content/uploads/2010/05/ADNI2_GE_3T_22.0_T2.pdf) were collected. Forty-six separate images were acquired for each DWI scan: 5 T2-weighted images with no dedicated diffusion sensitization (b_0 images) and 41 DWIs (b = 1000 seconds/mm^2). The DWI protocol for ADNI was chosen after a detailed evaluation of different protocols that could be performed in a reasonable amount time; we reported results of these comparisons previously (Jahanshad et al., 2010; Zhan et al., 2012a). All T1-weighted MRIs and DWIs were checked visually for quality assurance to exclude scans with excessive motion and/or artifacts after preprocessing corrections; all scans were included.

2.2. Image preprocessing

2.2.1. Preprocessing of baseline and 6-month follow-up anatomic scans

All extracerebral tissue was removed from both baseline and 6-month T1-weighted anatomic scans using a number of software packages, primarily ROBEX, a robust automated brain extraction program trained on manually "skull-stripped" MRI data (Iglesias et al., 2011), and FreeSurfer (Fischl et al., 2004). Skull-stripped volumes were visually inspected, and the best one was selected and further manually edited. Anatomic scans subsequently underwent intensity inhomogeneity normalization using the Montreal Neurologic Institute nu_correct tool (http://www.bic.mni.mcgill.ca/software/). To align data from different subjects into the same 3D coordinate space, each anatomic image was linearly aligned to a standard brain template (the Colin27, Holmes et al., 1998) using FSL FLIRT (Jenkinson et al., 2002).

2.2.2. Baseline DWI preprocessing

For each subject, all raw DWI volumes were aligned to the average b_0 image using the FSL eddy-correct tool (http://www.fmrib.ox.ac.

Table 1
Demographics and clinical scores for the participants

	e-MCI (n = 21)	l-MCI (n = 9)	p value for group difference
			e-MCI versus l-MCI
Age (y)	71.6 ± 8.1	72.1 ± 6.6	0.87
Sex	11 M/10 F	7 M/2 F	—
Education (y)	15.8 ± 2.7	16.2 ± 3.1	0.73
MMSE	27.9 ± 1.8	27.6 ± 1.7	0.63

Key: e-MCI, early mild cognitive impairment; F, females; l-MCI, late MCI; M, males; MMSE, Mini-Mental State Examination.

uk/fsl) to correct for head motion and eddy-current distortions. Nonbrain tissue was removed from the DWIs using the brain extraction tool from FSL (Smith, 2002). To correct for echo-planar–induced susceptibility artifacts, which can cause distortions at tissue-fluid interfaces, skull-stripped b_0 images were linearly aligned and then elastically registered to their respective baseline T1-weighted structural scans using an inverse consistent registration algorithm with a mutual information cost function (Leow et al., 2007). The resulting linear registration matrices and 3D deformation fields were then applied to the remaining 41 DWI volumes. Fractional anisotropy maps were subsequently calculated using FSL dtifit and overlaid on T1 anatomic scans to ensure proper alignment.

2.3. Fiber tractography

At each voxel, constant solid angle orientation distribution functions (CSA-ODFs) were computed using the normalized and dimensionless ODF estimator, derived for Q-ball imaging as in Aganj et al. (2010). The angular resolution of the ADNI data is somewhat limited to avoid long scan times that may tend to increase patient attrition, but the use of an CSA-ODF model makes best use of the available angular resolution. Tractography was performed on the linearly aligned sets of DWI volumes by probabilistically seeding voxels with a prior probability based on the fractional anisotropic value. Curves through a seed point received a score estimating the probability of the existence, computed from the ODFs. We used a voting process provided by the Hough transform to determine the best-fitting curves through each point (Fig. 1A, Aganj et al., 2011). Elastic deformations obtained from the echo-planar–induced distortion correction, mapping the average b_0 image to the T1-weighted image, were then applied to the resulting tracts' 3D coordinates. Each subject's dataset contained ~10,000 nonduplicated fibers (3D curves). In previous work, we have determined that this is a sufficient number of fibers to determine most of the common network topology measures accurately (Prasad et al., 2013a). We removed any erroneous fibers traced on the edge of the brain because of high-intensity noise. To limit small noisy tracts, we filtered out fibers with <10 points.

2.4. Automated cortical segmentation

Using FreeSurfer (http://surfer.nmr.mgh.harvard.edu/, Fischl et al., 2004), 34 cortical labels from the Desikan-Killiany atlas (Table 2, Desikan et al., 2006) were automatically extracted in each hemisphere from the raw baseline T1-weighted structural MRI scans. The T1-weighted images were then aligned to the corrected T1 images, and the linear transformation matrix was applied to the cortical parcellations using nearest neighbor interpolation (to avoid intermixing of labels). This placed the cortical labels in the same space as the tractography, calculated from the DWIs that were elastically registered to the corrected T1 space (Fig. 1B). To ensure tracts would intersect cortical labeled boundaries, labels were dilated with an isotropic box kernel of 5 × 5 × 5 voxels (Fig. 1C, Jahanshad et al., 2011a). Proper alignment of each subject's cortical parcellations, T1-weighted image, and tractography was verified by visually inspecting the 3 overlaid images.

2.5. N × N matrices representing structural connectivity

As in Jahanshad et al. (2011a), for each subject, a baseline 68 × 68 (34 right hemisphere labels and 34 left) connectivity matrix was created. Each element described the estimated proportion of the total number of fibers, in that subject, connecting each of the labels to each of the other labels (Fig. 1D).

2.6. Graph theory network analyses

We utilized the Brain Connectivity Toolbox (https://sites.google.com/site/bctnet/) and our weighted baseline connectivity matrices, to compute the measures whose values contribute to small-world architecture: CPL and MCC. In weighted measures, a path between two neighbors with strong connections contributes more than a path between two weakly connected neighbors. CPL is an average measure (across the whole network) of the minimum number of edges necessary to travel from one node to another in the network (i.e., average minimum path length, Watts and Strogatz, 1998). MCC is an average measure (across the whole network) of how many neighbors of a given node are also connected to each other, relative to the total possible number of connections in the network (Onnela et al., 2005). Small worldness, which measures the balance between network differentiation and network integration, is a ratio of the MCC and CPL of a network. As the small-worldness measure may falsely report small-world topology in highly segregated but poorly integrated networks (Rubinov and Sporns, 2010), we chose to assess MCC and CPL as joint predictors instead.

In a post hoc analysis, we additionally evaluated several weighted nodal measures to assess the extent to which local connectivity measures can also drive prediction: nodal CC, which parallels nodal EFF and nodal BTW centrality. The CC measures how many neighbors of a given node are also connected to each other,

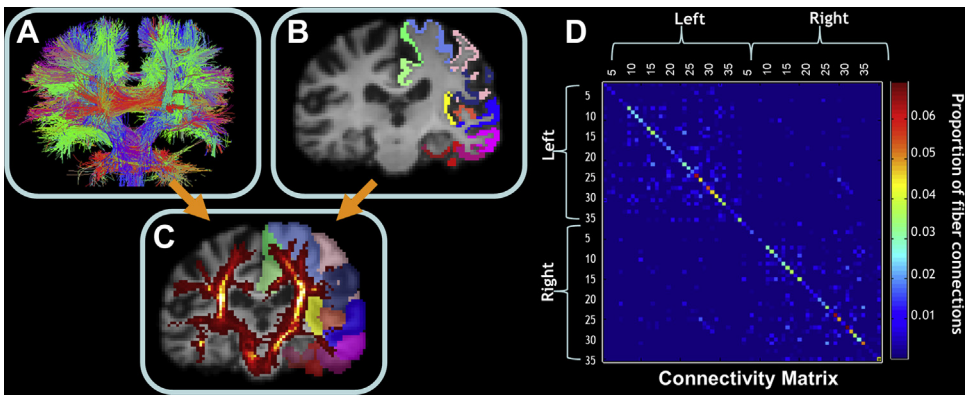

Fig. 1. (A) Echo-planar-induced distortion-corrected whole-brain tractography calculated from the diffusion-weighted image (DWI). (B) Anatomic cortical parcellations in one hemisphere are shown, registered to the same subject's DWI space. (C) Red fiber density map, where each voxel represents the total number of streamlines that pass through it, overlaid on the dilated labels. (D) Connectivity matrix, in which each colored element represents the proportion of detected fibers connecting each of the colored labels in each hemisphere to each of the other colored labels in (C), computed as a proportion of the total number of extracted fibers in the brain. This general method was used by us in Jahanshad et al. (2012a), to which the reader is referred for further details. (For interpretation of the references to color in this Figure, the reader is referred to the web version of this article.)

Table 2
Index of cortical labels extracted from the anatomic MRI scans by FreeSurfer

1	Banks of the superior temporal sulcus
2	Caudal anterior cingulate
3	Caudal middle frontal
4	NA
5	Cuneus
6	Entorhinal
7	Fusiform
8	Inferior parietal
9	Inferior temporal
10	Isthmus of the cingulate
11	Lateral occipital
12	Lateral orbitofrontal
13	Lingual
14	Medial orbitofrontal
15	Middle temporal
16	Parahippocampal
17	Paracentral
18	Pars opercularis
19	Pars orbitalis
20	Pars triangularis
21	Pericalcarine
22	Postcentral
23	Posterior cingulate
24	Precentral
25	Precuneus
26	Rostral anterior cingulate
27	Rostral middle frontal
28	Superior frontal
29	Superior parietal
30	Superior temporal
31	Supramarginal
32	Frontal pole
33	Temporal pole
34	Transverse temporal
35	Insula

Key: MRI, magnetic resonance imaging. Source: Fischl et al. (2004).

relative to the total possible connections, whereas the EFF of a node is the average inverse shortest path length calculated on the neighborhood of a given node. BTW is the fraction of all shortest paths in the network that contain a given node. Nodes with high values of BTW centrality participate in a large number of shortest paths. The equations to calculate each of these measures can be found in Rubinov and Sporns (2010).

2.7. Study-specific template creation

A study-specific minimal deformation template (MDT, Gutman et al., 2010) was created using 29 cognitively healthy elderly control subjects' baseline spatially aligned corrected anatomic volumes. Using a customized template from subjects in the study (rather than a standard atlas or a single optimally chosen subject) can reduce bias in the registrations. The MDT is the template that deviates least from the anatomy of the subjects, and, in some circumstances, it can improve statistical power (Lepore et al., 2007). The MDT was generated by creating an initial affine mean template from all 29 subjects and then registering all the aligned individual scans to that mean using a fluid registration (Leow et al., 2007) while regularizing the Jacobians (Yanovsky et al., 2007). A new mean was created from the registered scans; this process was iterated several times.

2.8. Tensor-based morphometry

To quantify 3D patterns of volumetric brain atrophy in MCI, each subject's 6-month preprocessed T1-weighted scan was elastically registered to its respective corrected baseline T1-weighted scan (Leow et al., 2007). A separate 3D Jacobian map (i.e., volumetric expansion factor map) was created for each subject to characterize the local volume differences between their baseline and 6-month scans. To ensure that the Jacobians had common anatomic coordinates for statistical analysis, each subject's respective 3D deformation field, from the elastic registration of the baseline T1-weighted scan to the MDT, was applied to each Jacobian map.

2.9. Statistics

We ran voxel-wise multiple linear regressions, covarying for sex and age, and a partial F test, using baseline MCC and CPL as predictors, both jointly and independently, of the longitudinal volumetric changes. Computing thousands of association tests at a voxel-wise level can introduce a high false-positive error rate in neuroimaging studies, if not corrected. To correct for these errors, we used the searchlight method for false discovery rate correction (Langers et al., 2007). All statistical maps are thresholded at a corrected p value to show regression coefficients only in regions that controlled the false discovery rate ($q = 0.05$).

In post hoc analyses, we further ran voxel-wise linear regressions, covarying for sex and age, to detect any associations between baseline CC (i.e. EFF) and BTW in each of the 68 nodes and the Jacobian maps. To correct for multiple comparisons for each of the 68 nodes, we used the searchlight method for false discovery rate correction at $q = 0.05/68$ or $q = 0.00074$ (Langers et al., 2007).

3. Results

We found a significant association between the baseline global network measures, CPL and MCC, used together as predictors in the same regression model, and 3D volumetric changes over the 6-month follow-up interval (Fig. 2A, corrected $p < 0.05$, Langers et al., 2007). Separately, MCC was significantly negatively associated with CSF volume changes surrounding the frontal, parietal, temporal, and occipital lobes and positively associated with regional volumetric changes around the right angular gyrus, left posterior orbital gyrus, left precuneus, and left fusiform (Fig. 2B). CPL was negatively associated with regional volume changes in the right and left anterior corona radiata, left superior corona radiata, left fusiform, and temporal lobe (Fig. 2C). This suggests that lower MCC and increased CPL at baseline are associated with decreases in tissue volume and increases in CSF expansion (implying tissue loss) in these regions after 6 months.

In a post hoc analysis, we also found that the right pars opercularis (inferior frontal gyrus) node's local EFF and CC were significantly positively associated with right internal capsule and temporal lobe and negatively associated with the right insular sulcus/lateral fissure and chiasmatic cistern (Fig. 3A, corrected $p < 0.00074$, Langers et al., 2007). The left superior parietal node's EFF and CC were significantly negatively associated with CSF volume around the left and right frontal lobes extending toward the right temporal lobe (Fig. 3B, corrected $p < 0.00074$, Langers et al., 2007). CC of the left pericalcarine node was negatively associated with CSF volume around the left frontal lobe (Fig. 3C, corrected $p < 0.00074$, Langers et al., 2007). Finally, the right temporal pole's BTW was positively associated with the volume of the left temporal lobe, angular gyrus, and posterior corona radiata (Fig. 3D, corrected $p < 0.00074$, Langers et al., 2007). Overall, these measures suggest that decreased local CC/EFF and BTW at baseline are associated with atrophy between baseline and a follow-up scan 6 months later.

4. Discussion

There is a great interest in predicting which subjects with MCI are likely to decline and in understanding what patterns of organizational decline in the brain may be harbingers of brain tissue

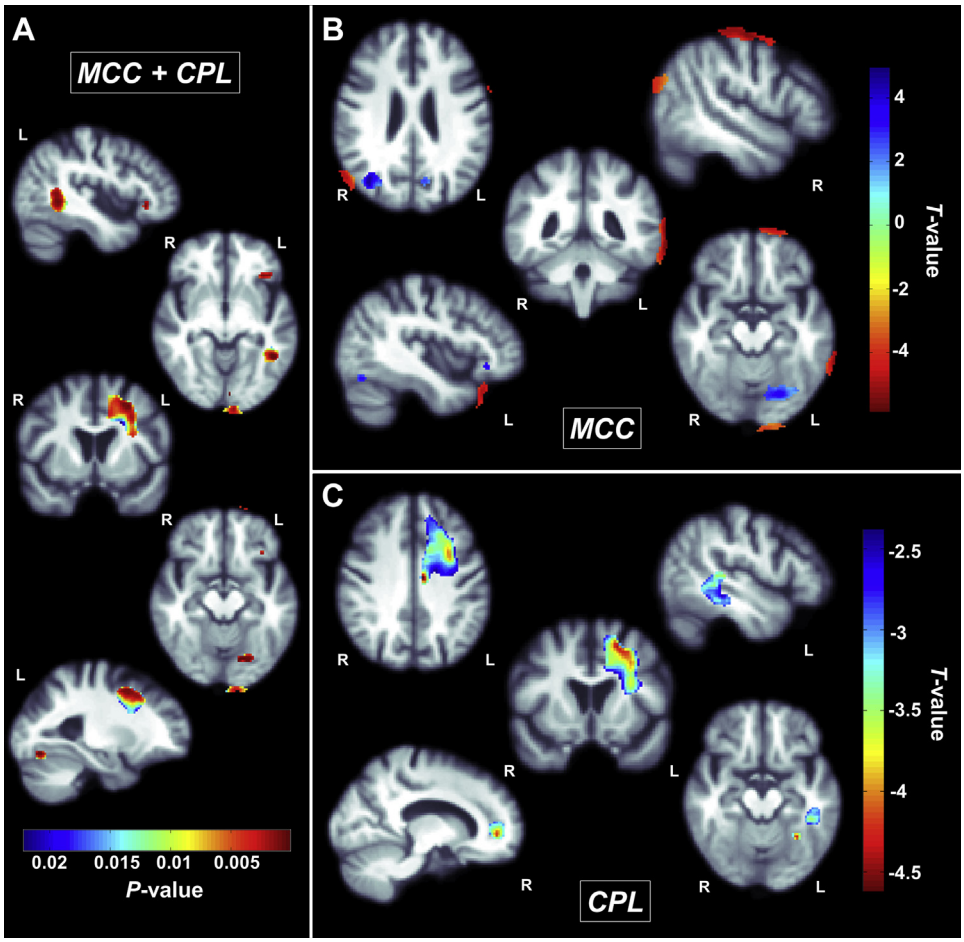

Fig. 2. (A) These p maps show regions where characteristic path length (CPL) and mean clustering coefficient (MCC) are joint predictors of volumetric changes on standard anatomic magnetic resonance images between baseline and a 6-month follow-up scan (corrected $p < 0.05$, Langers et al., 2007). (B) These maps show T values within regions where only MCC has a significant correlation with volumetric changes (corrected $p < 0.05$, Langers et al., 2007). (C) These maps show T values within regions where only CPL has a significant negative correlation with volumetric changes (corrected $p < 0.05$, Langers et al., 2007). Lower MCC and higher CPL at baseline are associated with greater volumetric atrophy after 6 months.

loss. Rather than evaluating gross anatomic structures of the brain independently, brain connectivity analyses can evaluate how integrated each region is with others, and, thus, may be more sensitive to alterations in brain systems as a whole. Several recent studies have suggested that AD progression may involve a loss of small-world characteristics in the brain's structural and functional networks (He et al., 2008; Sanz-Arigita et al., 2010; Stam et al., 2007). This is consistent with theoretical notions that small-world topology may be functionally beneficial and efficient. In this study, we assessed whether abnormalities in small worldness, the balance between network segregation and network integration, at baseline were associated with volumetric brain decline over a 6-month period.

We found an association between baseline small-world global network measures and volumetric changes in T1-weighted structural scans. Moreover, we found that lower MCC and higher CPL at baseline are associated with greater atrophy. Networks with lower CPL, reflecting speed or ease of functional integration of distributed brain regions, and higher levels of clustering or dense connections within regions across the network (MCC), may indicate a more functionally coherent neural system (Bullmore and Sporns, 2009).

To further investigate which regions or nodes may be driving global MCC associations, we assessed nodal clustering (CC), which parallels local nodal EFF, and found that decreased clustering in the right pars opercularis, left superior parietal node, and left pericalcarine node was significantly associated with patterns of volumetric brain atrophy. To assess which nodes might help facilitate lower global CPL, we evaluated nodal BTW centrality, which measures whether a node participates in a large number of shortest paths, facilitating integration between anatomically unconnected regions. We found that lower BTW in the right temporal pole was associated with atrophy.

These regions have been implicated in other DWI network studies. The superior parietal cortex, for example, is known to be affected by AD pathology early on (Jacobs et al., 2012), and is one of few "rich-club" hubs, the set of most highly interconnected nodes that play a central role in global network integration (van den Heuvel et al., 2012). A DTI study by Lo et al. (2010) also revealed nodal EFF reductions in several prefrontal areas including the orbital part of the inferior frontal gyrus and the temporal pole. In a connectivity study involving gray-matter volume correlations, the temporal pole, fusiform, cingulate, superior parietal region, and orbital frontal gyrus showed significant changes in the interregional correlations between normal control and AD groups (Yao et al., 2010).

This study could be extended in several ways. There is a great deal of work in brain connectivity analyses trying to identify subnetworks that are more sensitive to picking up differences in disease. Rather than pick a fixed partition of the cortical surface, other

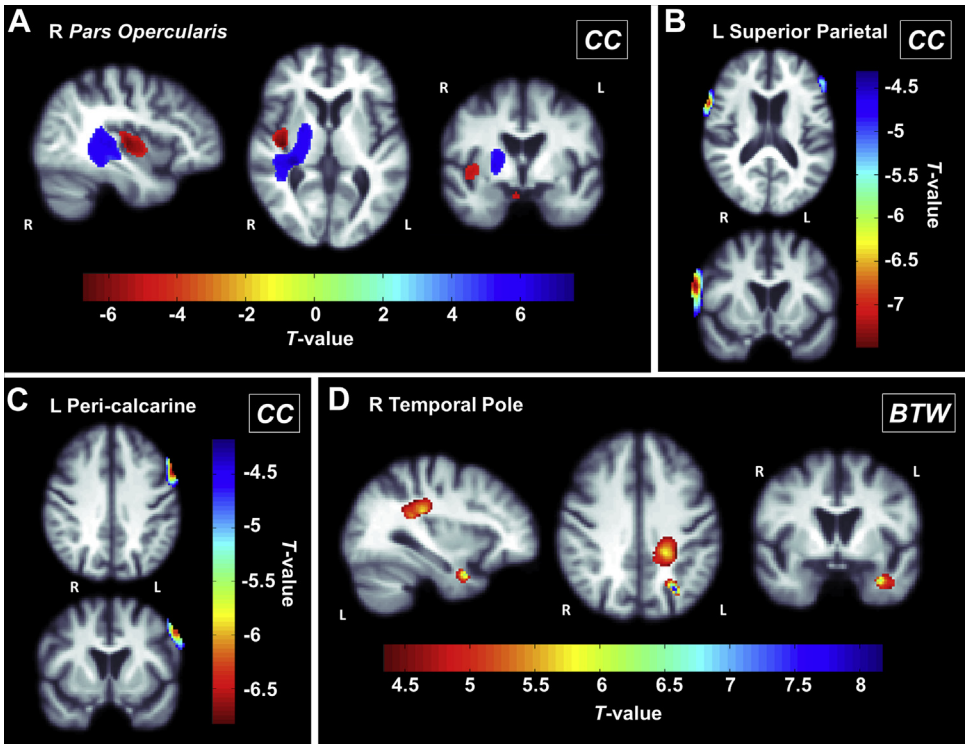

Fig. 3. Nodal clustering coefficient (CC) in the (A) right pars opercularis (inferior frontal gyrus), (B) left superior parietal node, and (C) left pericalcarine node are significantly associated with 3-dimensional patterns of volumetric brain atrophy, implying that increased clustering in these regions is associated with greater future atrophy. These same patterns are associated with efficiency (EFF) in these nodes, a measure that parallels CC. (D) Right temporal pole betweenness (BTW) centrality is positively associated with volume. These maps show *T* values within regions that show a significant association (corrected $p < 0.00074$, Langers et al., 2007).

work has attempted to adaptively refine and alter the cortical partition to better sensitize the analysis to group differences in disease (Prasad et al., 2013b). Although such adaptive approaches are elegant, they have the limitation that the cortical connectivity matrices from different studies and cohorts would be quite difficult to compare, as they are not defining connectivity for the same regions of interest. A second line of work has argued that connectivity can be defined in different ways, some of which may be better sensitized to pick up disease-related differences. For instance, some have defined lattice networks where every voxel is considered connected to all its immediate neighbors, and the angular diffusion signal at each voxel is used to define a dense-weighted network that is amenable to connectivity analysis (Li et al., 2013, unpublished data). Other approaches use statistical methods to preselect fibers likely to show associations with disease (Jahanshad et al., 2012b). A third line of work has attempted to threshold the connectivity networks to focus on nodes that have very high connectivity to others or that might be important hubs or highly connected "centers" for the network as a whole. This leads to concepts such as network filtrations, *k* cores, and rich-club coefficients (Dennis et al., 2013), which have begun to be tested for DTI-based analysis of connectivity in disease (Daianu et al., 2013a, 2013b, 2014). When the ADNI2 dataset is much larger, it should be possible to compare many of these methods head to head.

How the raw data have been acquired and processed, before any statistical analysis, can have large effects on results as each step is susceptible to sources of error and bias (Jones and Cercignani, 2010). For example, connectivity studies comparing networks derived from 3- and 7-T scans have revealed differences between field strengths (Zhan et al., 2012b). Additional limitations may include the limited angular resolution of the ADNI dataset, selected to avoid long scan times that may increase patient attrition. However, the use of an ODF model makes best use of the available angular resolution. The standard single-tensor model is somewhat limited in regions with extensive fiber crossing and mixing, whereas the ODF model can better resolve multifiber trajectories.

TBM voxel-wise analyses assume that a specific voxel location in the brain is identical across all subjects. However, registration accuracy from one subject to another may vary, in particular in aging studies where structures atrophy. Similarly, although tracts were corrected for susceptibility-induced artifacts, remaining distortion could cause misalignment and can lead to spurious results (Jahanshad et al., 2011b).

Different parcellation schemes may also affect graph theory metrics. We used the FreeSurfer Desikan-Killiany atlas (Desikan et al., 2006) for cortical parcellation, which has been widely used for structural connectivity analysis (Daianu et al., 2013a, 2013b, 2014; Hagmann et al., 2010; Honey et al., 2009). However, other parcellations are possible, and there is still work being done to understand how different parcellation templates and resolutions may influence different kinds of network measures (Bassett et al., 2011; Hagmann et al., 2010; Prasad et al., 2013b, unpublished data; Zalesky et al., 2010).

It appears that the degree of integration both across distributed brain regions, CPL and BTW, and locally within regions, MCC and CC, is an important indication of a coherent neural system at baseline and may be predictive of future decline. These results are preliminary and need to be replicated as ADNI2 progresses and new subjects are scanned. As the longitudinal study progresses, we can later investigate which of these subjects eventually develops AD and if these early aberrations in connectivity can help to predict a patient's conversion to AD, future brain tissue loss, and cognitive decline. This study offers evidence that DTI-based network measures may be a novel predictor of AD progression.

Disclosure statement

The authors have no potential, financial, or personal conflicts of interest including relationships with other people or organizations within 3 years of beginning the work submitted that could inappropriately influence this work. One of the authors, MWW, receives private funding unrelated to the content of this article.

Acknowledgements

Algorithm development and image analysis for this study were funded, in part, by grants to PT from the National Institute of Biomedical Imaging and Bioengineering (NIBIB) (R01 EB008281 and R01 EB008432), the National Institute on Aging (NIA), NIBIB, National Institute of Mental Health, the US National Library of Medicine, and the National Center for Research Resources (AG016570, AG040060, EB01651, MH097268, LM05639, and RR019771 to PT). Data collection and sharing for this project were funded by Alzheimer's Disease Neuroimaging Initiative (ADNI) (National Institutes of Health [NIH] grant U01 AG024904). ADNI is funded by the NIA, the NIBIB, and through contributions from the following: Abbott, Alzheimer's Association, Alzheimer Drug Discovery Foundation, Amorfix Life Sciences Ltd, AstraZeneca, Bayer Healthcare, BioClinica, Inc, Biogen Idec Inc, Bristol-Myers Squibb Company, Eisai Inc, Elan Pharmaceuticals Inc, Eli Lilly and Company, F. Hoffmann-La Roche Ltd, and its affiliated companies Genentech, Inc, GE Healthcare, Innogenetics, N.V., IXICO Ltd, Janssen Alzheimer Immunotherapy Research & Development, LLC, Johnson & Johnson Pharmaceutical Research & Development LLC, Medpace, Inc, Merck & Co, Inc, Meso Scale Diagnostics, LLC, Novartis Pharmaceuticals Corporation, Pfizer Inc, Servier, Synarc Inc, and Takeda Pharmaceutical Company. The Canadian Institutes of Health Research is providing funds to support ADNI clinical sites in Canada. Private sector contributions are facilitated by the Foundation for the NIH. The grantee organization is the Northern California Institute for Research and Education, and the study is coordinated by the Alzheimer's Disease Cooperative Study at the University of California, San Diego. ADNI data are disseminated by the Laboratory for Neuro Imaging at the University of Southern California. This research was also supported by NIH grants P30 AG010129 and K01 AG030514 from the National Institute of General Medical Sciences.

References

Achard, S., Bullmore, E., 2007. Efficiency and cost of economical brain functional networks. PLoS Comput. Biol. 3, e17.

Aganj, I., Lenglet, C., Sapiro, G., Yacoub, E., Ugurbil, K., Harel, N., 2010. Reconstruction of the orientation distribution function in single- and multiple-shell q-ball imaging within constant solid angle. Magn. Reson. Med. 64, 554–566.

Aganj, I., Lenglet, C., Jahanshad, N., Yacoub, E., Thompson, P.M., Sapiro, G., 2011. A Hough transform global probabilistic approach to multiple-subject diffusion MRI tractography. Med. Image Anal. 15, 414–425.

Bartzokis, G., 2011. Alzheimer's disease as homeostatic responses to age-related myelin breakdown. Neurobiol. Aging 32, 1341–1371.

Bassett, D.S., Brown, J.A., Deshpande, V., Carlson, J.M., Grafton, S.T., 2011. Conserved and variable architecture of human white matter connectivity. Neuroimage 54, 1262–1279.

Braak, H., Braak, E., 1996. Development of Alzheimer-related neurofibrillary changes in the neocortex inversely recapitulates cortical myelogenesis. Acta Neuropathol. 92, 197–201.

Braskie, M.N., Jahanshad, N., Stein, J.L., Barysheva, M., McMahon, K.L., de Zubicaray, G.I., Martin, N.G., Wright, M.J., Ringman, J.M., Toga, A.W., Thompson, P.M., 2011. Common Alzheimer's disease risk variant within the CLU gene affects white matter microstructure in young adults. J. Neurosci. 31, 6764–6770.

Brown, J.A., Terashima, K.H., Burggren, A.C., Ercoli, L.M., Miller, K.M., Small, G.W., Bookheimer, S.Y., 2011. Brain network local interconnectivity loss in aging APOE-4 allele carriers. Proc. Natl. Acad. Sci. U. S. A. 108, 20760–20765.

Bruscoli, M., Lovestone, S., 2004. Is MCI really just early dementia? A systematic review of conversion studies. Int. Psychogeriatr 16, 129–140.

Bullmore, E., Sporns, O., 2009. Complex brain networks: graph theoretical analysis of structural and functional systems. Nat. Rev. Neurosci. 10, 186–198.

Daianu, M., Jahanshad, N., Nir, T.M., Toga, A.W., Jack, C.R., Weiner, M.W., Thompson, P.M., for ADNI, 2013a. Breakdown of brain connectivity between normal aging and Alzheimer's disease: a structural k-core network analysis. Brain Connect. 3, 407–422.

Daianu, M., Dennis, E.L., Nir, T.M., Jahanshad, N., Toga, A.W., Jack, C.R., Weiner, M.W., Thompson, P.M., for ADNI, 2013b. Alzheimer's disease disrupts rich club organization in brain connectivity networks. Proc. IEEE Int. Symp. Biomed. Imaging, 266–269.

Daianu, M., Dennis, E.L., Jahanshad, N., Nir, T.M., Toga, A.W., Jack, C.R., Weiner, M.W., Thompson, P.M., 2014. Disrupted Brain Connectivity in Alzheimer's Disease: Effects of Network Thresholding. MICCAI Computational Diffusion MRI and Brain Connectivity 2014, 199–208.

Delbeuck, X., Van der Linden, M., Collette, F., 2003. Alzheimer's disease as a disconnection syndrome? Neuropsychol. Rev. 13, 79–92.

Dennis, E.L., Jahanshad, N., Toga, A.W., McMahon, K.L., de Zubicaray, G.I., Hickie, I., Wright, M.J., Thompson, P.M., 2013. Development of the "rich club" in brain connectivity networks from 438 adolescents and adults aged 12 to 30. Proc IEEE Int. Symp. Biomed. Imaging, 624–627.

Desikan, R.S., Segonne, F., Fischl, B., Quinn, B.T., Dickerson, B.C., Blacker, D., Buckner, R.L., Dale, A.M., Maguire, R.P., Hyman, B.T., Albert, M.S., Killiany, R.J., 2006. An automated labeling system for subdividing the human cerebral cortex on MRI scans into gyral based regions of interest. Neuroimage 31, 968–980.

Fischl, B., van der Kouwe, A., Destrieux, C., Halgren, E., Segonne, F., Salat, D.H., Busa, E., Seidman, L.J., Goldstein, J., Kennedy, D., Caviness, V., Makris, N., Rosen, B., Dale, A.M., 2004. Automatically parcellating the human cerebral cortex. Cereb. Cortex 14, 11–22.

Gutman, B., Svarer, C., Leow, A.D., Yanovsky, I., Toga, A.W., Thompson, P.M., 2010. Creating Unbiased Minimal Deformation Templates for Brain Volume Registration. OHBM, Barcelona, Spain.

Hagmann, P., Cammoun, L., Gigandet, X., Meuli, R., Honey, C.J., Wedeen, V.J., Sporns, O., 2008. Mapping the structural core of human cerebral cortex. PLoS Biol. 6, e159.

Hagmann, P., Sporns, O., Madan, N., Cammoun, L., Pienaar, R., Wedeen, V.J., Meuli, R., Thiran, J.-P., Grant, P.E., 2010. White matter maturation reshapes structural connectivity in the late developing human brain. Proc. Natl. Acad. Sci. USA 107, 19067–19072.

He, Y., Chen, Z., Evans, A., 2008. Structural insights into aberrant topological patterns of large-scale cortical networks in Alzheimer's disease. J. Neurosci. 28, 4756–4766.

Hilgetag, C.C., Burns, G.A., O'Neill, M.A., Scannell, J.W., Young, M.P., 2000. Anatomical connectivity defines the organization of clusters of cortical areas in the macaque and the cat. Phil. Trans. R. Soc. Lond. B Biol. Sci. 355, 91–110.

Holmes, C.J., Hoge, R., Collins, L., Woods, R., Toga, A.W., Evans, A.C., 1998. Enhancement of MR images using registration for signal averaging. J. Comput. Assist. Tomogr. 22, 324–333.

Honey, C.J., Sporns, O., Cammoun, L., Gigandet, X., Thiran, J.P., Meuli, R., Hagmann, P., 2009. Predicting human resting-state functional connectivity from structural connectivity. Proc. Natl. Acad. Sci. U. S. A. 106, 2035–2040.

Hua, X., Hibar, D.P., Ching, C.R., Boyle, C.P., Rajagopalan, P., Gutman, B.A., Leow, A.D., Toga, A.D., Jack, A.D., Harvey, D., Weiner, M.W., Thompson, P.M., 2013. Unbiased tensor-based morphometry: improved robustness and sample size estimates for Alzheimer's disease clinical trials. Neuroimage 66, 648–661.

Iglesias, J.E., Liu, C.Y., Thompson, P.M., Tu, Z., 2011. Robust brain extraction across datasets and comparison with publicly available methods. IEEE Trans. Med. Imaging 30, 1617–1634.

Iturria-Medina, Y., Sotero, R.C., Canales-Rodríguez, E.J., Alemán-Gómez, Y., Melie-García, L., 2008. Studying the human brain anatomical network via diffusion-weighted MRI and Graph Theory. Neuroimage 40, 1064–1076.

Jacobs, H.I., van Boxtel, M.P., Jolles, J., Verhey, F.R., Uylings, H.B., 2012. Parietal cortex matters in Alzheimer's disease: an overview of structural, functional and metabolic findings. Neurosci. Biobehav. Rev. 36, 297–309.

Jahanshad, N., Zhan, L., Bernstein, M.A., Borowski, B., Jack, C.R., Toga, A.W., Thompson, P.M., 2010. Diffusion tensor imaging in seven minutes: Determining trade-offs between spatial and directional resolution. Proc. IEEE Int. Symp. Biomed. Imaging 2010, 1161–1164.

Jahanshad, N., Aganj, I., Lenglet, C., Joshi, A., Jin, Y., Barysheva, M., McMahon, K.L., Zubicaray, G.I., Martin, N.G., Wright, M.J., Toga, A.W., Sapiro, G., Thompson, P.M., 2011a. Sex differences in the human connectome: 4-Tesla high angular resolution diffusion tensor imaging (HARDI) tractography in 234 young adult twins. Proc. IEEE Int. Symp. Biomed. Imaging 2011, 939–943.

Jahanshad, N., Aganj, I., Lenglet, C., Sapiro, G., Toga, A.W., McMahon, K.L., de Zubicaray, G. I., Martin, N.G., Wright, M.J., Thompson, P.M., 2011b. 4-Tesla high angular resolution diffusion tractography analysis of the human connectome in 234 subjects: sex differences and EPI distortion effects. Proc. Intl. Soc. Mag. Reson. Med. 19.

Jahanshad, N., Valcour, V.G., Nir, T.M., Kohannim, O., Busovaca, E., Nicolas, K., Thompson, P.M., 2012a. Disrupted brain networks in the aging HIV+ population. Brain Connect. 2, 335–444.

Jahanshad, N., Nir, T.M., Jack, C.R., Weiner, M.W., Toga, A.W., Thompson, P.M., 2012b. Boosting power to associate brain connectivity measures and dementia severity using seemingly unrelated regression. MICCAI Novel Imaging Biomarkers for Alzheimer's Disease Workshop, 103–112.

Jenkinson, M., Bannister, P., Brady, J., Smith, S., 2002. Improved optimisation for the robust and accurate linear registration and motion correction of brain images. Neuroimage 17, 825–841.
Jones, D.K., Cercignani, M., 2010. Twenty-five pitfalls in the analysis of diffusion MRI data. NMR Biomed. 23, 803–820.
Langers, D.R., Jansen, J.F., Backes, W.H., 2007. Enhanced signal detection in neuroimaging by means of regional control of the global false discovery rate. Neuroimage 38, 43–56.
Leow, A.D., Yanovsky, I., Chiang, M.C., Lee, A.D., Klunder, A., Lu, A., Becker, J., Davis, S., Toga, A.W., Thompson, P.M., 2007. Statistical properties of Jacobian maps and the realization of unbiased large-deformation nonlinear image registration. IEEE Trans. Med. Imaging 26, 822–832.
Lepore, N., Brun, C.C., Pennec, X., Chou, Y.Y., Lopez, O.L., Aizenstein, H.J., Becker, J.T., Toga, A.W., Thompson, P.M., 2007. Mean template for tensor-based morphometry using deformation tensors. Med. Image Comput. Comput. Assist. Interv. 10, 826–833.
Lo, C.Y., Wang, P.N., Chou, K.H., Wang, J., He, Y., Lin, C.P., 2010. Diffusion tensor tractography reveals abnormal topological organization in structural cortical networks in Alzheimer's disease. J. Neurosci. 30, 16876–16885.
Onnela, J.P., Saramaki, J., Kertesz, J., Kaski, K., 2005. Intensity and coherence of motifs in weighted complex networks. Phys. Rev. E Stat. Nonlin. Soft Matter Phys. 71, 065103.
Pievani, M., de Haan, W., Wu, T., Seeley, W.W., Frisoni, G.B., 2011. Functional network disruption in the degenerative dementias. Lancet Neurol. 10, 829–843.
Petersen, R.C., Doody, R., Kurz, A., Mohs, R.C., Morris, J.C., Rabins, P.V., Ritchie, K., Rossor, M., Thal, L., Winblad, B., 2001. Current concepts in mild cognitive impairment. Arch. Neurol. 58, 1985–1992.
Prasad, G., Nir, T.M., Toga, A.W., Thompson, P.M., ADNI, 2013a. Tractography density and network measures in Alzheimer's disease. Proc. IEEE Int. Symp. Biomed. Imaging 2013, 692–695.
Prasad, G., Joshi, S., Toga, A.W., Thompson, P.M., 2013b. A dynamical clustering model of brain connectivity inspired by the n-body problem. Multimodal Brain Image Analysis Lecture Notes in Computer Science 8159, 129–137.
Reijneveld, J.C., Ponten, S.C., Berendse, H.W., Stam, C.J., 2007. The application of graph theoretical analysis to complex networks in the brain. Clin. Neurophysiol. 118, 2317–2331.
Rubinov, M., Sporns, O., 2010. Complex network measures of brain connectivity: uses and interpretations. Neuroimage 3, 1059–1069.
Sanz-Arigita, E.J., Schoonheim, M.M., Damoiseaux, J.S., Rombouts, S.A., Maris, E., Barkhof, F., Scheltens, P., Stam, C.J., 2010. Loss of 'small-world' networks in Alzheimer's disease: graph analysis of FMRI resting-state functional connectivity. PLoS One 5, e13788.
Smith, S.M., 2002. Fast robust automated brain extraction. Hum. Brain Mapp. 17, 143–155.
Stam, C.J., Jones, B.F., Nolte, G., Breakspear, M., Scheltems, P.H., 2007. Small-world networks and functional connectivity in Alzheimer's disease. Cereb. Cortex 17, 92–99.
Toga, A.W., Thompson, P.M., 2013. Connectomics sheds new light on Alzheimer's disease. Biol. Psychiatry 73, 390–392.
van den Heuvel, M.P., Kahn, R.S., Goni, J., Sporns, O., 2012. High-cost, high-capacity backbone for global brain communication. Proc. Natl. Acad. Sci. U. S. A. 109, 11372–11377.
Watts, D.J., Strogatz, S.H., 1998. Collective dynamics of 'small-world' networks. Nature 393, 440–442.
Yanovsky, I., Thompson, P.M., Osher, S., Leow, A.D., 2007. Topology preserving log-unbiased nonlinear image registration: theory and implementation. IEEE Conference on Computer Vision and Pattern Recognition, 1–8.
Yao, Z., Zhang, Y., Lin, L., Zhou, Y., Xu, C., Jiang, T., 2010. Abnormal cortical networks in mild cognitive impairment and Alzheimer's disease. PLoS Comput. Biol. 6, e1001006.
Zalesky, A., Fornito, A., Harding, I.H., Cocchi, L., Yücel, M., Pantelis, C., Bullmore, E., 2010. Whole-brain anatomical networks: does the choice of nodes matter? Neuroimage 50, 970–983.
Zhan, L., Jahanshad, N., Ennis, D.B., Jin, Y., Bernstein, M.A., Borowski, B.J., Jack Jr., C.R., Toga, A.W., Leow, A.D., Thompson, P.M., 2012a. Angular versus spatial resolution trade-offs for diffusion imaging under time constraints. Hum. Brain Mapp. 34, 2688–2706.
Zhan, L., Jahanshad, N., Jin, Y., Lenglet, C., Mueller, B.A., Sapiro, G., Ugurbil, K., Harel, N., Toga, A.W., Lim, K.O., Thompson, P.M., 2012b. Field strength effects on diffusion measures and brain connectivity networks. Brain Connect. 3, 72–86.